JACS
JOURNAL OF THE AMERICAN CHEMICAL SOCIETY
Article
pubs.acs.org/JACS

The Realistic Domain Structure of As-Synthesized Graphene Oxide from Ultrafast Spectroscopy

Qun Zhang,*[,†,‡] Hongjun Zheng,[‡] Zhigang Geng,[†,§] Shenlong Jiang,[†] Jing Ge,[‡] Kaili Fan,[‡] Sai Duan,[∥] Yang Chen,[†,‡] Xiaoping Wang,[†,§] and Yi Luo*[,†,‡,∥]

[†]Hefei National Laboratory for Physical Sciences at the Microscale, [‡]Department of Chemical Physics, and [§]Department of Physics, University of Science and Technology of China, Hefei, Anhui 230026, China

[∥]Department of Theoretical Chemistry and Biology, School of Biotechnology, Royal Institute of Technology, AlbaNova, S-106 91 Stockholm, Sweden

Supporting Information

ABSTRACT: Graphene oxide (GO) is an attractive alternative for large-scale production of graphene, but its general structure is still under debate due to its complicated nonstoichiometric nature. Here we perform a set of femtosecond pump−probe experiments on as-synthesized GO to extrapolate structural information *in situ*. Remarkably, it is observed that, in these highly oxidized GO samples, the ultrafast graphene-like dynamics intrinsic to pristine graphene is completely dominant over a wide energy region and can be modified by the localized impurity states and the electron−phonon coupling under certain conditions. These observations, combined with the X-ray photoelectron spectroscopy analysis and control experiments, lead to an important conclusion that GO consists of two types of domain, namely the carbon-rich graphene-like domain and the oxygen-rich domain. This study creates a new understanding of the realistic domain structure and properties of as-synthesized GO, offering useful guidance for future applications based on chemically modified/functionalized graphenes.

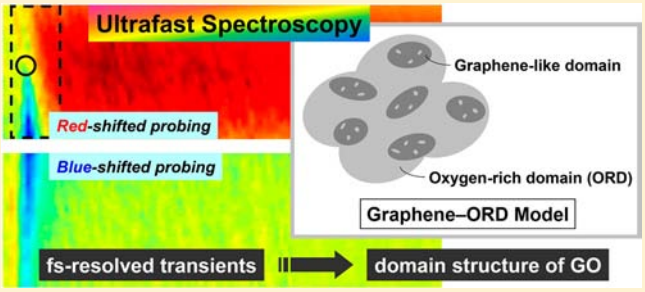

INTRODUCTION

In recent years graphene oxide (GO) has attracted great attention, which was initially due to its potential in mass production of graphene.[1−4] It was then realized that the rich chemistry provided by the oxidation groups on GO is, in fact, very useful for functionalization of graphene.[5−8] Although a variety of possible oxidation groups on GO have been identified by, e.g., X-ray photoelectron spectroscopy (XPS),[9] the realistic domain structure of GO (i.e., how these oxidation groups are distributed on GO) is still under debate due to its complicated nonstoichiometric nature.[5,6,10]

Currently, the oxidation groups are basically considered to be distributed on the graphene substrate of GO in a random fashion—small (a few nm), ordered sp^2 clusters randomly isolated within the sp^3 C−O matrix.[5,11] Such a graphene−matrix model (Figure 1a) implies that GO will no longer preserve the unique linear band structure of graphene,[1,2] opening the band gap as a result of the significant distortion or buckling of the hexagonal lattice caused by C−O bonds.[12] Depending on the oxidation level, the band gap could be as large as 2.7−3.1 eV, a typical energy range for amorphous carbon.[13] Just from the perspective of general chemistry, however, it is conceivable that another distinctly different structural model may exist, in which the highly oxidized, as-synthesized GO consists of two types of domain: the carbon-rich graphene-like domain (i.e., oxidatively hybridized graphene sheet with much larger size than the randomly distributed nm-sized sp^2 clusters) and the large-area oxygen-rich domain (ORD). As GO is a very poor conductor, it is more likely to exist as densely packed ORDs with small graphene island inclusions (oxidatively hybridized), as schematically depicted in Figure 1b. Note that other forms of oxygen on graphene, such as graphene monoxide,[14] may be present in small quantities in the as-synthesized GO, making it a very complex system.

In the context of the graphene−ORD model (Figure 1b), it can be expected that the graphene-like domain possesses a rather small band gap due to weak oxygen doping,[15] while a large energy gap is present in between the low-lying electron-occupied states and the high-lying electron-unoccupied states of the ORD. Apparently, this new domain structural model of GO should lead to rather different properties (as well as functionalities) with respect to the graphene−matrix model.

Direct visualization of the domain structure of GO can be achieved via scanning tunneling microscopy (STM)[16] or atomic force microscopy (AFM), but often with ambiguity even if the resolution is quite high. The standard spectroscopic tools such as Raman and XPS, although could provide useful structural information, are difficult to distinguish between the afore-

Received: July 11, 2013
Published: July 29, 2013

   dx.doi.org/10.1021/ja407110r | J. Am. Chem. Soc. 2013, 135, 12468−12474

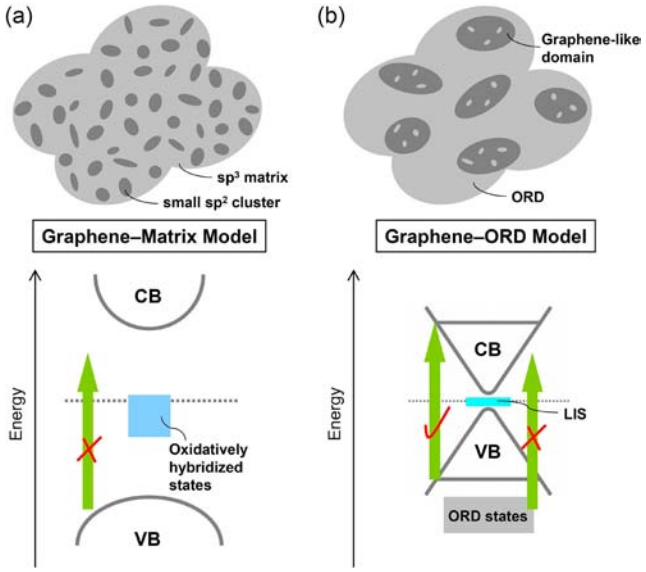

Figure 1. Schematic illustration of the two GO models (along with pertinent band structures): (a) graphene–matrix and (b) graphene–ORD models. VB, valence band; CB, conduction band; LIS, localized impurity states. Note that the high-lying electron-unoccupied ORD states are not depicted here. Note also that the weak oxygen doping in the graphene-like domain may induce a slight shifting of the Fermi level (along the Dirac point of graphene),[1,2] which is not specifically depicted here. Refer to Supporting Information for more insights (from our first-principles calculations) into the electronic structure of GO at different oxidation levels.

mentioned two structural models of GO. One thus needs to find an alternative method to overcome the difficulty.

Here, we perform a set of femtosecond (fs) pump–probe experiments on the as-synthesized GO samples in an attempt to extrapolate *in situ* the realistic domain structural information of GO. Essentially, detailed analysis of the observed extraordinary carrier dynamics in GO validates the new graphene–ORD model.

EXPERIMENTAL SECTION

GO Sample Preparation. The as-synthesized GO samples (mostly single-layered GO flakes with a lateral size of ~45 μm on average) were prepared using a modified Hummers method[17−19] (refer to Supporting Information for detailed procedures). These GO samples are highly oxidized with an atomic C:O ratio of ~2.7:1 (see discussion later). It should be pointed out that, to avoid any unwanted doping influence by supported substrate that may adversely affect the carrier dynamics of interest, the as-synthesized GO samples were dispersed in pure deionized water to form stable suspensions (1.5 mg/mL) instead of being grown or coated on substrates.

Time-Resolved Pump–Probe Experiments. In our ultrafast measurements performed on a 25 fs Ti:sapphire laser system, a nondegenerate, visible pump–white-light (WL) probe strategy was implemented (details in Supporting Information). The pump wavelengths were chosen to be in 500–650 nm, ensuring that the single-photon energy (1.9–2.5 eV) is most likely only sufficient to excite the graphene-like domain provided the graphene–ORD model is valid. On the other hand, since the pulsed pump laser with peak intensities higher than 40 GW/cm^2 could lead to reduction of GO, we adopted a peak intensity of ~25 GW/cm^2. Negligible C:O ratio changes were found before and after each measurement, as confirmed by XPS characterization. Importantly, such a moderate intensity is far too low to induce nonlinear two-photon absorption processes that are energetically allowed even in the ORD. This has been verified by a recent degenerate (800 nm) fs pump–probe study under high-intensity excitation (typically ~270 GW/cm^2).[20]

RESULTS AND DISCUSSION

Among a large amount of transient absorption data collected on freshly prepared GO, we show here a typical set (Figure 2) that

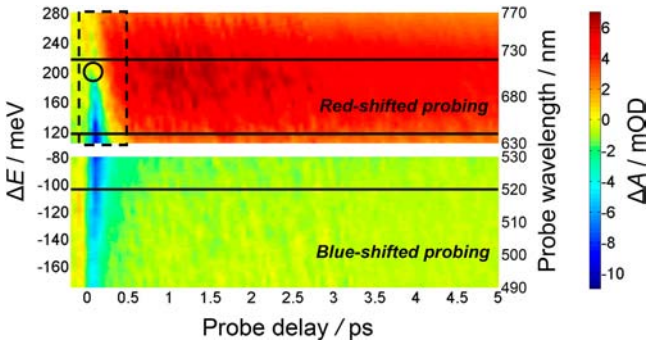

Figure 2. Contour plot showing the full transient absorption data recorded on the highly oxidized, as-synthesized GO (C:O ≈ 2.7:1) samples using a 570 nm pump and a WL probe. ΔA, the pump-induced absorbance changes; positive (negative) ΔA values point to enhanced (reduced) absorption of the probing light. Positive (negative) probe delays mean that the probe pulse follows (precedes) the pump pulse. OD, optical density; ΔE, half the energy difference of the pump and probe photons; positive (negative) ΔE implies that the probe is red (blue)-shifted with respect to the pump. Refer to the text for details regarding the cut lines, dashed box, and open circle.

was registered with a 570 nm pump and a WL probe (490–530 and 630–770 nm). In this contour plot, the pump-induced transient absorbance change of the probing light, ΔA (in mOD; OD, optical density), is plotted as functions of probe delay and probe wavelength. Note that, for the sake of discussion that follows, we here bring in an energy coordinate, ΔE, designating half the energy difference of the pump and probe photons, $(\hbar\omega_{pump} - \hbar\omega_{probe})/2$.

Extraordinary Graphene-Like Dynamics Revealed via Blue-Shifted Probing. Given the graphene–ORD model, it can be expected that the localized impurity states (LIS) at around the Fermi level (light-blue bar in Figure 1b and hereafter) would not affect the carrier dynamics if one uses a blue-shifted probing scheme. This is understandable because the pump-generated valence-band (VB) holes (including the low-energy tail of their Fermi–Dirac distribution inside VB) will set a blockade (Figure 3a) to effectively impede electron transfer from the LIS to where the probe monitors (outside the blockade). Such a blockade effect is automatically mandated by the momentum conservation as a result of the symmetric linear band structure of graphene[1,2] despite a small band gap opening in the graphene-like domain. In light of this expectation, we started with a probe scan in the blue-shifted region.

Indeed, we observed complete graphene-type transients (type I hereafter) over a wide blue-shifted region of 490–530 nm (Figure 2, lower panel). As normally observed in pristine graphene,[21−28] this type of ΔA transients manifests itself as probe bleach ($\Delta A < 0$), which is well understood as a consequence of the so-called phase-state filling or more commonly Pauli blocking (PB) effect.[21] Figure 3b shows a typical kinetic trace probed at 520 nm (corresponding to the lower cut line in Figure 2). A biexponential fit yields two recovery time constants, $\tau_1 = 106 \pm 13$ fs and $\tau_2 = 1.1 \pm 0.2$ ps,

dx.doi.org/10.1021/ja407110r | J. Am. Chem. Soc. 2013, 135, 12468−12474

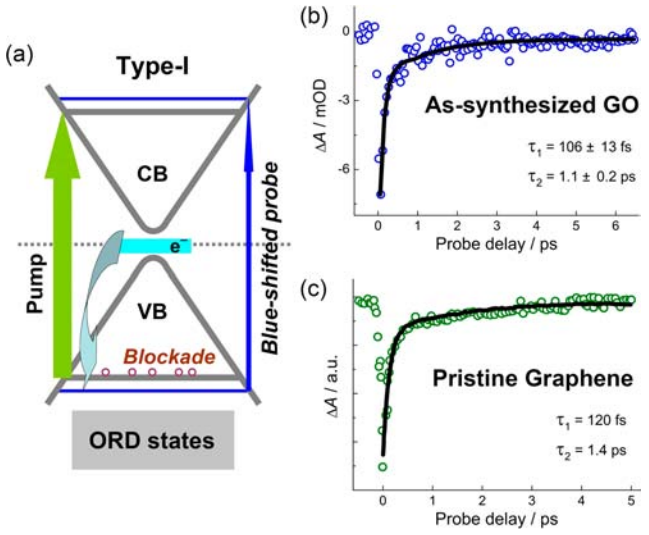

Figure 3. (a) Schematic illustration of VB-hole blockade effect responsible for the type I graphene-like dynamics observed in highly oxidized, as-synthesized GO under blue-shifted probing. (b) Typical type I kinetics, extracted from the line cutting at 520 nm in Figure 2. (c) Representative kinetics observed in pristine graphene (data adapted from ref 21).

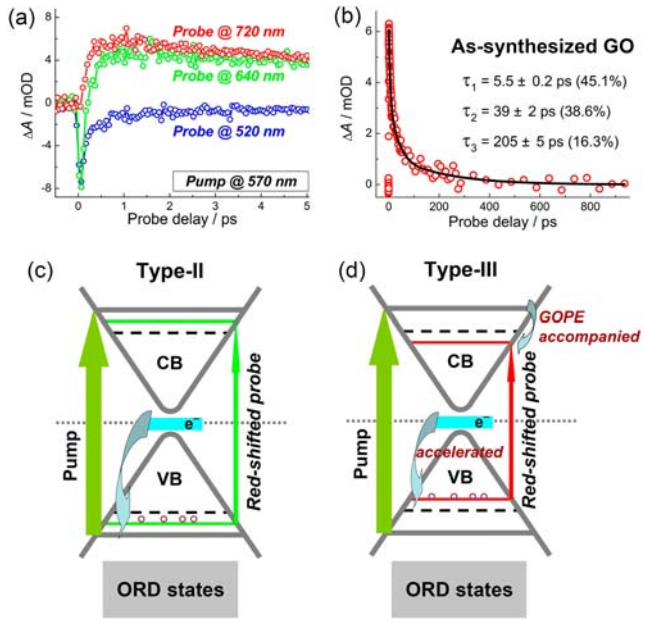

Figure 4. (a) Typical types II (green) and III (red) kinetics, extracted from the lines cutting at 640 and 720 nm in Figure 2, respectively. The type I data shown in Figure 3b are replotted here (blue) for comparison. (b) Full data (extended to ~1 ns) corresponding to the red trace in (a). The pertinent mechanisms are schematically illustrated in (c) and (d); refer to the text for detailed discussion.

on the same time scales as their counterparts for graphene[21−28] as well as reduced GO (rGO).[29,30] As a comparison, a representative kinetic trace observed in pristine graphene (data adapted from ref 21) is plotted in Figure 3c. It should be stressed here that the observed type I kinetics turned out to be independent of the pump wavelength (500−650 nm), which nicely conforms to the fact that the aforementioned blockade effect (Figure 3a) should not depend on where the pump is applied as long as a blue-shifted probing scheme is used.

This finding indicates that within the highly oxidized, as-synthesized GO does exist isolated graphene-like domain that essentially preserves the intrinsic electronic properties of graphene, thereby providing direct *in situ* evidence for the validity of the graphene−ORD model of GO. We notice that a recent study on reversible electrical reduction and oxidation of GO has also revealed the segregation of graphene and graphene oxide in partially reduced GO films,[31] and theoretical predictions about segregation can be found in literature.[32,33] Here, our ultrafast spectroscopic study enables identification of segregation even in freshly prepared GO samples.

Rich Dynamics Fully Mapped out via Red-Shifted Probing. As the probe scan was extended to a red-shifted region of 630−700 nm, a new type of transients (denoted type II) was observed. A typical kinetic trace probed at 640 nm is shown in Figure 4a (green; corresponding to the middle cut line in Figure 2). Obviously, the dip in the initial time window closely resembles that of the type I kinetics (blue; reproduced from Figure 3b for comparison); probe bleach still dominates herein. However, right after this narrow window (~250 fs in width) a ΔA sign reversal occurs.

The more pronounced distinction lies in the subsequent long time recovery, in sharp contrast to the much shorter one for the type I kinetics. Such a slow recovery, certainly not attributable to the PB effect that governs the graphene or graphene-like dynamics (in light of the reversed ΔA sign), must be connected to the surface trap states provided by the electron-rich oxidation groups on GO. In fact, electron detrapping from the surface trap states of GO (and rGO) has been verified as a very slow process.[34] Nevertheless, on the basis of our explicit observation of the type I kinetics, we can safely rule out the low-lying electron-occupied ORD states as the origin of the type II kinetics. This is amenable to reason because no energetically favorable pathways are open for promoting electrons from these ORD states (refer to Figure 1b); if otherwise, the type I graphene-like dynamics would by no means dominate over a wide energy region.

Then, let us turn to the near-Fermi-level LIS. Unlike the blue-shifted probing case, the blockade set by the pump-generated VB holes does not take effect in this case, simply because where the red-shifted probe monitors energetically falls within the blockade (Figure 4c). Therefore, the LIS electrons that rapidly fill into the pump-generated VB holes (obeying the Fermi−Dirac distribution) will definitely contribute to the ΔA signals in such a way that the probe absorption gets enhanced. As observed, such an electron−hole transfer process appears rather efficient; right after the initial window as narrow as ~250 fs, the contributions from the enhanced probe absorption ($\Delta A > 0$) prevail over those from the persisting probe bleach ($\Delta A < 0$). For a strongly bonded system with right orbital matching, such a fast electron transfer (assisted with strong electronic coupling) is not unusual.

Further scanning the probe into a redder region of 700−770 nm revealed a third type of transients (denoted type III). A typical kinetic trace probed at 720 nm is also shown in Figure 4a (red; corresponding to the upper cut line in Figure 2). Here exclusively positive ΔA signals show up. Interestingly, except for the vanished initial dip, it follows nearly the same recovery as the type II kinetics. A multiexponential fit to the full data (Figure 4b) yields three recovery time constants: $\tau_1 = 5.5 \pm 0.2$ ps, $\tau_2 = 39 \pm 2$ ps, and $\tau_3 = 205 \pm 5$ ps.

Mechanism Underlying Kinetics Changeover. How to interpret such kind of kinetics switching under red-shifted probing? To answer this, care must be taken in the initial time

dx.doi.org/10.1021/ja407110r | J. Am. Chem. Soc. 2013, 135, 12468−12474

window marked by a dashed box in Figure 2, within which one can clearly see a critical changeover (marked by an open circle) between the two types of kinetics along the wavelength (or energy) coordinate. In terms of ΔE, the changeover occurs at ~200 meV, an energy nicely coinciding with that of the G-mode optical phonon emission (GOPE) normally observed in graphene (typically ~196 meV)[35] and in our GO samples as well (refer to Supporting Information for Raman G-band signature at ~1600 cm^{-1} ≈ 200 meV). It should be emphasized that this finding is not limited only to the 570 nm pump case. An additional case study that uses a 500 nm pump is exemplified in Figure 5, from which the critical kinetics changeover at $\Delta E \approx 200$ meV can be clearly identified (marked with a white open circle).

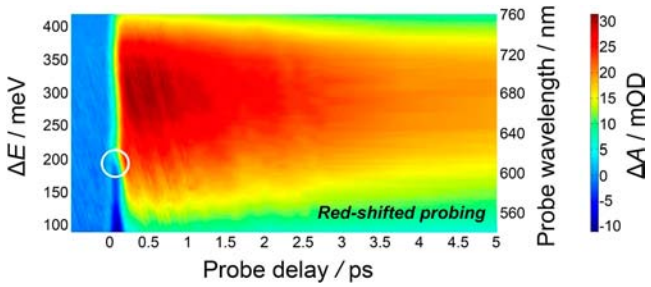

Figure 5. Further manifestation of GOPE in the GO (C:O ≈ 2.7:1) samples, in which the transient absorption data were recorded with a 500 nm pump and a red-shifted WL probe in 540–760 nm. Refer to Figure 2 for relevant annotations.

To understand how this kinetics changeover correlates to the GOPE in GO, one may take into account the fact that the Raman G mode is known as the most dominant phonon mode in graphene-like materials.[36] As schematically depicted in Figure 4c,d, the black dashed line (nominally marking $\Delta E \approx$ 200 meV) splits the CB below where the pump reaches (upper gray solid line) into two zones. The event that the pump-excited hot electrons in the CB rapidly redistribute into the lower zone is expected to be accompanied by emission of at least one G-mode optical phonon when $\Delta E > 200$ meV (Figure 4d, upper curved arrow), rendering this particular zone a GOPE-active one. As the GOPE stands with the $C(sp^2)$–$C(sp^2)$ stretch vibrations, the strong electron–vibration (or vibronic) coupling in the graphene-like domain will inevitably result in acceleration of electron transfer from the LIS to the pump-generated VB holes (Figure 4d, lower curved arrow). It is this accelerated electron–hole transfer that causes the probe-bleach contributions to be completely suppressed even within the initial time window. On the contrary, however, the upper zone is GOPE-inactive ($\Delta E < 200$ meV; Figure 4c), whereby the PB effect governs within the initial time window until the electron–hole transfer takes over, giving rise to the type II kinetics featuring a zero crossing of ΔA.

Coexistence of Ultrafast and Ultraslow Dynamics. We have revealed the unique coexistence of ultrafast and ultraslow dynamics in the same highly oxidized, as-synthesized GO samples. In terms of the type I kinetics, its characteristic recovery (τ_1 ~100 fs and τ_2 ~1 ps), as in pristine graphene, should be responsible for the cooling of quasi-equilibrium carriers via carrier–(optical) phonon scattering (on the time scale of a few hundred fs) and the final arrival of equilibrium carrier–(acoustic) phonon scattering (on a longer time scale of a few ps), respectively.[26] On the other hand, the type II/III kinetics exhibit much slower carrier cooling: a few, a few tens, and a few hundreds of ps. The charge carrier diffusion in GO is hindered along the graphene-like sheet mainly due to the surface defects (trap sites), thereby facilitating energy relaxation through alternate pathways such as carrier–phonon scattering and carrier trapping.[34] Among the three sizable components (portion percentages given in Figure 4b), the fastest one can be assigned to electron–(acoustic) phonon interaction,[29,34] while the other two should originate from much slower detrapping of the trapped electrons in different trap depths.[34] Here, the missing of the sub-ps component implies no significant percolation from the oxygen-rich domain to the graphene-like domain, which also supports the graphene–ORD model. It is worth noting that we have mapped out the dynamics of the pronounced vibronic coupling in the highly oxidized GO, which is, however, verified as connected to the graphene-like domain of GO. This interesting finding can be regarded as collateral evidence for the extensive, strong electron–phonon interactions in graphene and, in turn, could be beneficial for understanding the electrical and optoelectronic properties of other graphene-like materials.

In terms of the crossover from ultrafast to ultraslow dynamics in GO, it should be pointed out that a recent electrochemical study has revealed similar wavelength-dependent crossover behavior in GO,[37] where the optical absorption of the samples was found to be switchable from ultrafast saturable absorption to slower nonlinear absorption reversibly depending on the wavelength and degree of the reduction. This has been related with simultaneous presence of GO and graphene-like domains in partially reduced GO and hence can be considered the precedent of our observations presented here. Note also that such kind of crossover behavior was also discussed in epitaxial graphene in which similar effects were observed even without any GO domains (which may still be present somehow).[22] The explanation was based on doping, rather than the presence of GO or impurity bands. The doping effect, in the current case, can be regarded as a minor perturbation, if any. As stated before, to avoid any unwanted doping influence by supported substrate that may adversely affect the carrier dynamics of interest, the GO samples under investigation were dispersed in pure deionized water to form stable suspensions instead of being grown or coated on substrates. Nevertheless, as GO is a very complex system, if it is grown or coated on substrates (e.g., SiC),[22] multiple effects including doping (charges transferred from the substrate) and GO-related band modifications (as reported here) are most likely in play concomitantly to account for the observed crossover behavior.

Further Evidence for Graphene–ORD Model. It is known that GO can be effectively reduced by ultraviolet (UV) irradiation.[38,39] We have then focused a fs UV (400 nm) laser with a peak intensity of ~250 GW/cm^2 (an order of magnitude higher than that used in our pump–probe measurements) onto the original as-synthesized GO suspensions. Long-time (~20 h) irradiation produced *in situ* the rGO sample. Figure 6 shows the C1s XPS spectra of the two samples, both of which were directly collected from the solution without any chemical separation treatments.

The XPS spectrum for the original GO sample can be well decomposed into four bands, peaking at (1) 284.4, (2) 286.5, (3) 287.1, and (4) 288.0 eV, respectively (Figure 6a). The band (1) originates from carbon atoms forming C–C/C=C bonds, while the bands (2), (3), and (4) are associated with several types of oxidation groups, as annotated within the plot. The

dx.doi.org/10.1021/ja407110r | J. Am. Chem. Soc. 2013, 135, 12468–12474

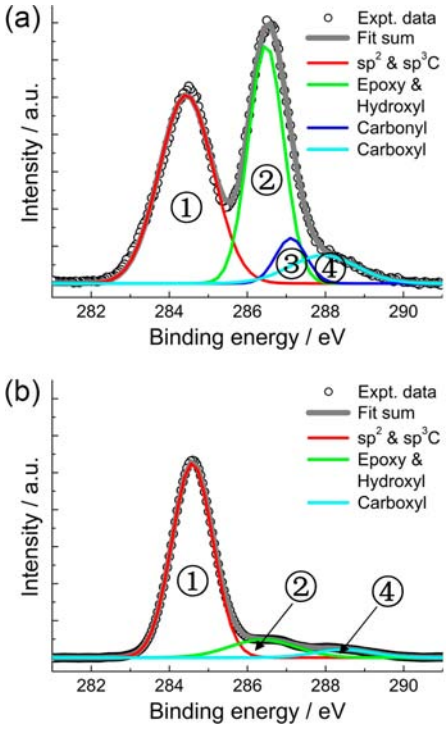

Figure 6. C1s XPS spectra of (a) the original as-synthesized GO (C:O ≈ 2.7:1) sample and (b) the rGO (C/O ≈ 10.6:1) sample that was produced *in situ* by long-time UV-laser irradiation.

above spectral assignments agree well with the previous reports[40−42] as well as our recent first-principles study on binding energy of C1s orbital in GO.[9] From the relative areas of these bands, 1:0.832:0.137:0.186 for (1):(2):(3):(4), the atomic C:O ratio is determined to be ∼2.7:1, consistent with the documented values for as-synthesized GO.[40−42] Notably, however, the spectrum for the rGO sample can only be well fitted with three components (Figure 6b); efforts to decompose it into more than three components turned out to yield meaningless results. The three decomposed bands peak at 284.6, 286.4, and 288.5 eV, respectively, corresponding to the bands (1), (2), and (4) for GO (Figure 6a) albeit the band (4) blue-shifts by 0.5 eV for some reason. The relative band areas are 1:0.150:0.058 [(1):(2):(4)], pointing to a much larger C:O ratio of ∼10.6:1. This indicates that the UV-irradiated reduction is quite effective in removing most oxidation groups on GO, especially the epoxy and hydroxyl groups; the band (2) drops off by a factor of ∼5.5, while the band (4) by ∼3.2. Of particular interest is the vanished band (3). As this band arises from the carbonyl groups, the observation of its utter disappearance strongly suggests that the weakly bonded carbonyl groups on GO should be the preferential targets of the UV-irradiated reduction. Consequently, the LIS—mainly contributed from the carbonyl groups in the graphene-like domain of GO (refer to Supporting Information for the relevant discussion based on our first-principles calculations)—can be predicted to be vastly removed by the UV-irradiated reduction in this case.

To verify the above prediction, we have also performed pump−probe measurements on this *in situ* produced and intactly collected rGO sample. Figure 7a shows a typical kinetic trace recorded with a 400 nm pump (back to the moderate peak intensity of ∼25 GW/cm^2) and a 640 nm probe. Interestingly, although obtained under red-shifted probing, it

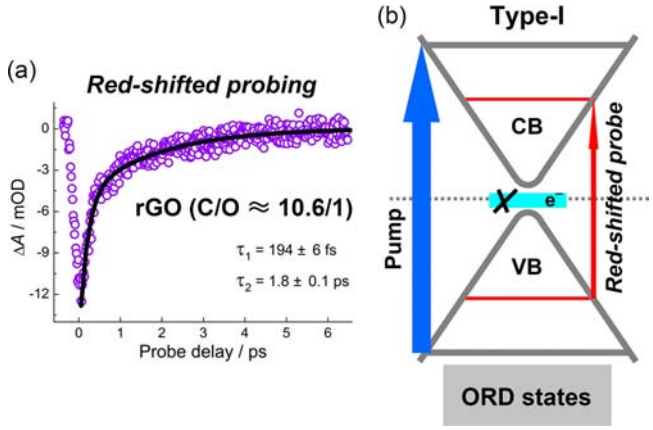

Figure 7. (a) Transient kinetics observed in rGO (C:O ≈ 10.6:1) with a 400 nm pump and a 640 nm probe. (b) With the electron−hole transfer channels being eliminated, the PB effect accounts for the observed type I graphene-like dynamics under the red-shifted probe.

turns out to be nearly identical to the type I kinetics observed for the original GO sample under blue-shifted probing (Figure 3b). It should be pointed out that such an observation was found to be independent of the pump wavelength and the probing scheme. Evidently, the LIS that play a key role in controlling the extraordinary dynamics in the original GO sample must have been, to a large extent, eliminated for this rGO sample (Figure 7b); if otherwise, the opening of the LIS electron−VB hole transfer channels would definitely not let the net type I kinetics, as shown in Figure 7a, dominate under red-shifted probing. Therefore, this set of control experiments has, in turn, further evidenced the validity of the graphene−ORD model.

In terms of the C:O ratio of the GO and rGO samples, it is interesting to note that a very recent work addressed the room-temperature metastability of multilayer GO films.[43] According to this work, at room temperature multilayer GO is a metastable material undergoing spontaneous chemical modifications and reduction with a relaxation time of ∼35 days (e.g., at day 1 the C:O ratio of their GO samples was found to be ∼2.27:1 while at day 40 changed to ∼2.63:1).[43] During the course of each run of our ultrafast measurements (roughly one month), the C:O ratio (∼2.7:1) of our as-synthesized GO samples may have also undergone such kind of variation, which however turned out not to affect the carrier dynamics we observed; in other words, the reproducibility of our pump−probe data was quite high. It is also worth noting that the quite large, ∼10.6:1, C:O ratio of our rGO samples was found to attain only after a long-time UV irradiation.

Last but not least, we notice that a two-layer structural model of as-synthesized GO was recently suggested, in which two distinct components, the large, covalently functionalized graphene-like sheet and the small, highly oxidative debris, are considered noncovalently complexed together.[44] Despite being commensurate in spirit with the graphene−ORD model, such a model seems not reconcilable with our UV-reduction tests. It is conceivable that under intense UV exposure, the oxidative debris could leave the graphene-like sheet due to the noncovalent binding between them but are difficult to be reduced due to their compact structures.[44] If this is the case, the condensed sample collected from the solution without any chemical separation treatments would maintain a large number of oxygen atoms, and then it seems unlikely for us to attain *in*

dx.doi.org/10.1021/ja407110r | J. Am. Chem. Soc. 2013, 135, 12468−12474

situ the large C:O ratio of ~10.6:1. We also notice that a recent STM examination[16] echoes well to the graphene–ORD model. From the STM images of GO, it was observed that the hexagonal lattice of the GO sheets (i.e., graphene-like domain) is partially preserved, while the oxygen-rich domain lacking ordered lattice features appears distinguishable from pristine graphene by the appearance of bright spots/regions.[16] Along the same line, we anticipate that future ultrahigh-resolution microscopic investigations would be highly beneficial for gleaning more realistic structural information about GO, e.g., the nature of interdomain percolation and defects on the graphene substrate of GO.

CONCLUSION

With a set of femtosecond pump–probe experiments featuring a thorough probe scan (blue- and red-shifted with respect to the pump), in conjunction with the XPS analysis and control experiments, the present work reveals *in situ* the realistic domain structure of as-synthesized GO, in which two types of domain, the carbon-rich graphene-like domain and the oxygen-rich domain, are verified to coexist. We envision that the established GO model may lay down the foundation for advancing technological applications of GO as well as other chemically modified/functionalized graphenes in different fields. Furthermore, the unique coexistence of ultrafast and ultraslow carrier dynamics in as-synthesized GO, together with the elucidated mechanisms involving electron–hole transfer and electron–phonon coupling, would be of instructive value for a better understanding of the electrical and optoelectronic properties of other graphene-type materials.

ASSOCIATED CONTENT

Supporting Information

Insights from the first-principles calculations, details of the GO sample preparation and characterizations, and details of the femtosecond pump–probe experiments and data processing. This material is available free of charge via the Internet at http://pubs.acs.org.

AUTHOR INFORMATION

Corresponding Author

qunzh@ustc.edu.cn; luo@kth.se

Notes

The authors declare no competing financial interest.

ACKNOWLEDGMENTS

This work was jointly supported by the NBRPC (2010CB923300), the NSFC (21173205, 91127042, and 20925311), and the CAS (XDB01020000 and KJCX2-EW-W09). Partial support from the FRFCUC (WK2340000012) and the USTC-NSRL Joint Funds (KY2340000021) is also acknowledged.

REFERENCES

(1) Geim, A. K.; Novoselov, K. S. *Nat. Mater.* **2007**, *6*, 183–191.
(2) Geim, A. K. *Science* **2009**, *324*, 1530–1534.
(3) Park, S.; Ruoff, R. S. *Nat. Nanotechnol.* **2009**, *4*, 217–224.
(4) Dikin, D. A.; Stankovich, S.; Zimney, E. J.; Piner, R. D.; Dommett, G. H. B.; Evmenenko, G.; Nguyen, S. T.; Ruoff, R. S. *Nature* **2007**, *448*, 457–460.
(5) Loh, K. P.; Bao, Q. L.; Eda, G.; Chhowalla, M. *Nat. Chem.* **2010**, *2*, 1015–1024.
(6) Dreyer, D. R.; Park, S.; Bielawski, C. W.; Ruoff, R. S. *Chem. Soc. Rev.* **2010**, *39*, 228–240.
(7) Stankovich, S.; Dikin, D. A.; Dommett, G. H. B.; Kohlhaas, K. M.; Zimney, E. J.; Stach, E. A.; Piner, R. D.; Nguyen, S. T.; Ruoff, R. S. *Nature* **2006**, *442*, 282–286.
(8) Eda, G.; Chhowalla, M. *Adv. Mater.* **2010**, *22*, 2392–2415.
(9) Zhang, W. H.; Carravetta, V.; Li, Z. Y.; Luo, Y.; Yang, J. L. *J. Chem. Phys.* **2009**, *131*, 244505.
(10) Szabó, T.; Berkesi, O.; Forgó, P.; Josepovits, K.; Sanakis, Y.; Petridis, D.; Dékány, I. *Chem. Mater.* **2006**, *18*, 2740–2749.
(11) Erickson, K.; Erni, R.; Lee, Z.; Alem, N.; Gannett, W.; Zettl, A. *Adv. Mater.* **2010**, *22*, 4467–4472.
(12) Mkhoyan, K. A.; Contryman, A. W.; Silcox, J.; Stewart, D. A.; Eda, G.; Mattevi, C.; Miller, S.; Chhowalla, M. *Nano Lett.* **2009**, *9*, 1058–1063.
(13) Mathioudakis, C.; Kopidakisb, G.; Keliresc, P. C.; Patsalasa, P.; Giotia, M.; Logothetidisa, S. *Thin Solid Films* **2005**, *482*, 151–155.
(14) Mattson, E. C.; Pu, H.; Cui, S.; Schofield, M. A.; Rhim, S.; Lu, G.; Nasse, M. J.; Ruoff, R. S.; Weinert, M.; Gajdardziska-Josifovska, M.; Chen, J.; Hirschmugl, C. J. *ACS Nano* **2011**, *5*, 9710–9717.
(15) Eda, G.; Lin, Y.-Y.; Mattevi, C.; Yamaguchi, H.; Chen, H.-A.; Chen, I.-S.; Chen, C.-W.; Chhowalla, M. *Adv. Mater.* **2010**, *22*, 505–509.
(16) Gómez-Navarro, C.; Weitz, R. T.; Bittner, A. M.; Scolari, M.; Mews, A.; Burghard, M.; Kern, K. *Nano Lett.* **2007**, *7*, 3499–3503.
(17) Hammers, W. S.; Offeman, R. E. *J. Am. Chem. Soc.* **1958**, *80*, 1339–1339.
(18) Wilson, N. R.; Pandey, P. A.; Beanland, R.; Young, R. J.; Kinloch, I. A.; Gong, L.; Liu, Z.; Suenaga, K.; Rourke, J. P.; York, S. J.; Sloan, J. *ACS Nano* **2009**, *3*, 2547–2556.
(19) Kosynkin, D. V.; Higginbotham, A. L.; Sinitskii, A.; Lomeda, J. R.; Dimiev, A.; Price, B. K.; Tour, J. M. *Nature* **2009**, *458*, 872–876.
(20) Liu, Z.-B.; Zhao, X.; Zhang, X.-L.; Yan, X.-Q.; Wu, Y.-P.; Chen, Y.-S.; Tian, J.-G. *J. Phys. Chem. Lett.* **2011**, *2*, 1972–1977.
(21) Dawlaty, J. M.; Shivaraman, S.; Chandrasekhar, M.; Rana, F.; Spencer, M. G. *Appl. Phys. Lett.* **2008**, *92*, 042116.
(22) Sun, D.; Wu, Z.-K.; Divin, C.; Li, X.; Berger, C.; de Heer, W. A.; First, P. N.; Norris, T. B. *Phys. Rev. Lett.* **2008**, *101*, 157402.
(23) Newson, R. W.; Dean, J.; Schmidt, B.; van Driel, H. M. *Opt. Express* **2009**, *17*, 2326–2333.
(24) Wang, H.; Strait, J. H.; George, P. A.; Shivaraman, S.; Shields, V. B.; Chandrashekhar, M.; Hwang, J.; Rana, F.; Spencer, M. G. *Appl. Phys. Lett.* **2010**, *96*, 081917.
(25) Shang, J.; Luo, Z.; Cong, C.; Lin, J.; Yu, T.; Gurzadyan, G. G. *Appl. Phys. Lett.* **2010**, *97*, 163103.
(26) Obraztsov, P. A.; Rybin, M. G.; Tyurnina, A. V.; Garnov, S. V.; Obraztsova, E. D.; Obraztsov, A. N.; Svirko, Y. P. *Nano Lett.* **2011**, *11*, 1540–1545.
(27) Shang, J.; Yu, T.; Lin, J.; Gurzadyan, G. G. *ACS Nano* **2011**, *5*, 3278–3283.
(28) Gao, B.; Hartland, G.; Fang, T.; Kelly, M.; Jena, D.; Xing, H.; Huang, L. *Nano Lett.* **2011**, *11*, 3184–3189.
(29) Kumar, S.; Anija, M.; Kamaraju, N.; Vasu, K. S.; Subrahmanyam, K. S.; Sood, A. K.; Rao, C. N. R. *Appl. Phys. Lett.* **2009**, *95*, 191911.
(30) Ruzicka, B. A.; Werake, L. K.; Zhao, H.; Wang, S.; Loh, K. P. *Appl. Phys. Lett.* **2010**, *96*, 173106.
(31) Ekiz, O. Ö.; Urel, M.; Güner, H.; Mizrak, A. K.; Dâna, A. *ACS Nano* **2011**, *5*, 2475–2482.
(32) Boukhvalov, D. W.; Katsnelson, M. I. *J. Am. Chem. Soc.* **2008**, *130*, 10697–10701.
(33) Yan, J.; Xian, L.; Chou, M. Y. *Phys. Rev. Lett.* **2009**, *103*, 086802.
(34) Kaniyankandy, S.; Achary, S. N.; Rawalekar, S. R.; Ghosh, H. N. *J. Phys. Chem. C* **2011**, *115*, 19110–19116.
(35) Faugeras, C.; Nerrière, A.; Potemski, M.; Mahmood, A.; Dujardin, E.; Berger, C.; de Heer, W. A. *Appl. Phys. Lett.* **2008**, *92*, 011914.
(36) Tse, W. K.; Hwang, E. H.; Sarma, S. D. *Appl. Phys. Lett.* **2008**, *93*, 023128.

(37) Kürüm, U.; Ekiz, O. Ö.; Yaglioglu, H. G.; Elmali, A.; Ürel, M.; Güner, H.; Mizrak, A. K.; Ortaç, B.; Dâna, A. *Appl. Phys. Lett.* **2011**, *98*, 141103.
(38) Ding, Y. H.; Zhang, P.; Zhuo, Q.; Ren, H. M.; Yang, Z. M.; Jiang, Y. *Nanotechnology* **2011**, *22*, 215601.
(39) Guardia, L.; Villar-Rodil, S.; Paredes, J. I.; Rozada, R.; Martínez-Alonso, A.; Tascón, J. M. D. *Carbon* **2012**, *50*, 1014−1024.
(40) Zhang, J.; Yang, H.; Shen, G.; Cheng, P.; Zhang, J.; Guo, S. *Chem. Commun.* **2010**, *46*, 1112−1114.
(41) Fan, Z.-J.; Kai, W.; Yan, J.; Wei, T.; Zhi, L.-J.; Feng, J.; Ren, Y.-M.; Song, L.-P.; Wei, F. *ACS Nano* **2011**, *5*, 191−198.
(42) Mei, X.; Ouyang, J. *Carbon* **2011**, *49*, 5389−5397.
(43) Kim, S.; Zhou, S.; Hu, Y.; Acik, M.; Chabal, Y. J.; Berger, C.; de Heer, W.; Bongiorno, A.; Riedo, E. *Nat. Mater.* **2012**, *11*, 544−549.
(44) Rourke, J. P.; Pandey, P. A.; Moore, J. J.; Bates, M.; Kinloch, I. A.; Young, R. J.; Wilson, N. R. *Angew. Chem., Int. Ed.* **2011**, *50*, 3173−3177.